BABAR -PUB-16/007
SLAC-PUB-17118

Measurement of the $D^*(2010)^+ - D^+$ mass difference

J. P. Lees,[1] V. Poireau,[1] V. Tisserand,[1] E. Grauges,[2] A. Palano,[3] G. Eigen,[4] D. N. Brown,[5] Yu. G. Kolomensky,[5] M. Fritsch,[6] H. Koch,[6] T. Schroeder,[6] C. Hearty[ab],[7] T. S. Mattison[b],[7] J. A. McKenna[b],[7] R. Y. So[b],[7] V. E. Blinov[abc],[8] A. R. Buzykaev[a],[8] V. P. Druzhinin[ab],[8] V. B. Golubev[ab],[8] E. A. Kravchenko[ab],[8] A. P. Onuchin[abc],[8] S. I. Serednyakov[ab],[8] Yu. I. Skovpen[ab],[8] E. P. Solodov[ab],[8] K. Yu. Todyshev[ab],[8] A. J. Lankford,[9] J. W. Gary,[10] O. Long,[10] A. M. Eisner,[11] W. S. Lockman,[11] W. Panduro Vazquez,[11] D. S. Chao,[12] C. H. Cheng,[12] B. Echenard,[12] K. T. Flood,[12] D. G. Hitlin,[12] J. Kim,[12] T. S. Miyashita,[12] P. Ongmongkolkul,[12] F. C. Porter,[12] M. Röhrken,[12] Z. Huard,[13] B. T. Meadows,[13] B. G. Pushpawela,[13] M. D. Sokoloff,[13] L. Sun,[13,*] J. G. Smith,[14] S. R. Wagner,[14] D. Bernard,[15] M. Verderi,[15] D. Bettoni[a],[16] C. Bozzi[a],[16] R. Calabrese[ab],[16] G. Cibinetto[ab],[16] E. Fioravanti[ab],[16] I. Garzia[ab],[16] E. Luppi[ab],[16] V. Santoro[a],[16] A. Calcaterra,[17] R. de Sangro,[17] G. Finocchiaro,[17] S. Martellotti,[17] P. Patteri,[17] I. M. Peruzzi,[17] M. Piccolo,[17] M. Rotondo,[17] A. Zallo,[17] S. Passaggio,[18] C. Patrignani,[18,†] H. M. Lacker,[19] B. Bhuyan,[20] U. Mallik,[21] C. Chen,[22] J. Cochran,[22] S. Prell,[22] H. Ahmed,[23] A. V. Gritsan,[24] N. Arnaud,[25] M. Davier,[25] F. Le Diberder,[25] A. M. Lutz,[25] G. Wormser,[25] D. J. Lange,[26] D. M. Wright,[26] J. P. Coleman,[27] E. Gabathuler,[27,‡] D. E. Hutchcroft,[27] D. J. Payne,[27] C. Touramanis,[27] A. J. Bevan,[28] F. Di Lodovico,[28] R. Sacco,[28] G. Cowan,[29] Sw. Banerjee,[30] D. N. Brown,[30] C. L. Davis,[30] A. G. Denig,[31] W. Gradl,[31] K. Griessinger,[31] A. Hafner,[31] K. R. Schubert,[31] R. J. Barlow,[32,§] G. D. Lafferty,[32] R. Cenci,[33] A. Jawahery,[33] D. A. Roberts,[33] R. Cowan,[34] S. H. Robertson,[35] B. Dey[a],[36] N. Neri[a],[36] F. Palombo[ab],[36] R. Cheaib,[37] L. Cremaldi,[37] R. Godang,[37,¶] D. J. Summers,[37] P. Taras,[38] G. De Nardo,[39] C. Sciacca,[39] G. Raven,[40] C. P. Jessop,[41] J. M. LoSecco,[41] K. Honscheid,[42] R. Kass,[42] A. Gaz[a],[43] M. Margoni[ab],[43] M. Posocco[a],[43] G. Simi[ab],[43] F. Simonetto[ab],[43] R. Stroili[ab],[43] S. Akar,[44] E. Ben-Haim,[44] M. Bomben,[44] G. R. Bonneaud,[44] G. Calderini,[44] J. Chauveau,[44] G. Marchiori,[44] J. Ocariz,[44] M. Biasini[ab],[45] E. Manoni[a],[45] A. Rossi[a],[45] G. Batignani[ab],[46] S. Bettarini[ab],[46] M. Carpinelli[ab],[46,**] G. Casarosa[ab],[46] M. Chrzaszcz[a],[46] F. Forti[ab],[46] M. A. Giorgi[ab],[46] A. Lusiani[ac],[46] B. Oberhof[ab],[46] E. Paoloni[ab],[46] M. Rama[a],[46] G. Rizzo[ab],[46] J. J. Walsh[a],[46] A. J. S. Smith,[47] F. Anulli[a],[48] R. Faccini[ab],[48] F. Ferrarotto[a],[48] F. Ferroni[ab],[48] A. Pilloni[ab],[48] G. Piredda[a],[48,‡] C. Bünger,[49] S. Dittrich,[49] O. Grünberg,[49] M. Heß,[49] T. Leddig,[49] C. Voß,[49] R. Waldi,[49] T. Adye,[50] F. F. Wilson,[50] S. Emery,[51] G. Vasseur,[51] D. Aston,[52] C. Cartaro,[52] M. R. Convery,[52] J. Dorfan,[52] W. Dunwoodie,[52] M. Ebert,[52] R. C. Field,[52] B. G. Fulsom,[52] M. T. Graham,[52] C. Hast,[52] W. R. Innes,[52] P. Kim,[52] D. W. G. S. Leith,[52] S. Luitz,[52] D. B. MacFarlane,[52] D. R. Muller,[52] H. Neal,[52] B. N. Ratcliff,[52] A. Roodman,[52] M. K. Sullivan,[52] J. Va'vra,[52] W. J. Wisniewski,[52] M. V. Purohit,[53] J. R. Wilson,[53] A. Randle-Conde,[54] S. J. Sekula,[54] M. Bellis,[55] P. R. Burchat,[55] E. M. T. Puccio,[55] M. S. Alam,[56] J. A. Ernst,[56] R. Gorodeisky,[57] N. Guttman,[57] D. R. Peimer,[57] A. Soffer,[57] S. M. Spanier,[58] J. L. Ritchie,[59] R. F. Schwitters,[59] J. M. Izen,[60] X. C. Lou,[60] F. Bianchi[ab],[61] F. De Mori[ab],[61] A. Filippi[a],[61] D. Gamba[ab],[61] L. Lanceri,[62] L. Vitale,[62] F. Martinez-Vidal,[63] A. Oyanguren,[63] J. Albert[b],[64] A. Beaulieu[b],[64] F. U. Bernlochner[b],[64] G. J. King[b],[64] R. Kowalewski[b],[64] T. Lueck[b],[64] I. M. Nugent[b],[64] J. M. Roney[b],[64] R. J. Sobie[ab],[64] N. Tasneem[b],[64] T. J. Gershon,[65] P. F. Harrison,[65] T. E. Latham,[65] R. Prepost,[66] and S. L. Wu[66]

(The *BABAR* Collaboration)

[1] *Laboratoire d'Annecy-le-Vieux de Physique des Particules (LAPP), Université de Savoie, CNRS/IN2P3, F-74941 Annecy-Le-Vieux, France*
[2] *Universitat de Barcelona, Facultat de Fisica, Departament ECM, E-08028 Barcelona, Spain*
[3] *INFN Sezione di Bari and Dipartimento di Fisica, Università di Bari, I-70126 Bari, Italy*
[4] *University of Bergen, Institute of Physics, N-5007 Bergen, Norway*
[5] *Lawrence Berkeley National Laboratory and University of California, Berkeley, California 94720, USA*
[6] *Ruhr Universität Bochum, Institut für Experimentalphysik 1, D-44780 Bochum, Germany*
[7] *Institute of Particle Physics[a]; University of British Columbia[b], Vancouver, British Columbia, Canada V6T 1Z1*
[8] *Budker Institute of Nuclear Physics SB RAS, Novosibirsk 630090[a], Novosibirsk State University, Novosibirsk 630090[b], Novosibirsk State Technical University, Novosibirsk 630092[c], Russia*
[9] *University of California at Irvine, Irvine, California 92697, USA*
[10] *University of California at Riverside, Riverside, California 92521, USA*
[11] *University of California at Santa Cruz, Institute for Particle Physics, Santa Cruz, California 95064, USA*

This material is based upon work supported by the U.S. Department of Energy, Office of Science, under Contract No. DE-AC02-76SF00515.

[12] California Institute of Technology, Pasadena, California 91125, USA
[13] University of Cincinnati, Cincinnati, Ohio 45221, USA
[14] University of Colorado, Boulder, Colorado 80309, USA
[15] Laboratoire Leprince-Ringuet, Ecole Polytechnique, CNRS/IN2P3, F-91128 Palaiseau, France
[16] INFN Sezione di Ferrara[a]; Dipartimento di Fisica e Scienze della Terra, Università di Ferrara[b], I-44122 Ferrara, Italy
[17] INFN Laboratori Nazionali di Frascati, I-00044 Frascati, Italy
[18] INFN Sezione di Genova, I-16146 Genova, Italy
[19] Humboldt-Universität zu Berlin, Institut für Physik, D-12489 Berlin, Germany
[20] Indian Institute of Technology Guwahati, Guwahati, Assam, 781 039, India
[21] University of Iowa, Iowa City, Iowa 52242, USA
[22] Iowa State University, Ames, Iowa 50011, USA
[23] Physics Department, Jazan University, Jazan 22822, Kingdom of Saudi Arabia
[24] Johns Hopkins University, Baltimore, Maryland 21218, USA
[25] Laboratoire de l'Accélérateur Linéaire, IN2P3/CNRS et Université Paris-Sud 11, Centre Scientifique d'Orsay, F-91898 Orsay Cedex, France
[26] Lawrence Livermore National Laboratory, Livermore, California 94550, USA
[27] University of Liverpool, Liverpool L69 7ZE, United Kingdom
[28] Queen Mary, University of London, London, E1 4NS, United Kingdom
[29] University of London, Royal Holloway and Bedford New College, Egham, Surrey TW20 0EX, United Kingdom
[30] University of Louisville, Louisville, Kentucky 40292, USA
[31] Johannes Gutenberg-Universität Mainz, Institut für Kernphysik, D-55099 Mainz, Germany
[32] University of Manchester, Manchester M13 9PL, United Kingdom
[33] University of Maryland, College Park, Maryland 20742, USA
[34] Massachusetts Institute of Technology, Laboratory for Nuclear Science, Cambridge, Massachusetts 02139, USA
[35] Institute of Particle Physics and McGill University, Montréal, Québec, Canada H3A 2T8
[36] INFN Sezione di Milano[a]; Dipartimento di Fisica, Università di Milano[b], I-20133 Milano, Italy
[37] University of Mississippi, University, Mississippi 38677, USA
[38] Université de Montréal, Physique des Particules, Montréal, Québec, Canada H3C 3J7
[39] INFN Sezione di Napoli and Dipartimento di Scienze Fisiche, Università di Napoli Federico II, I-80126 Napoli, Italy
[40] NIKHEF, National Institute for Nuclear Physics and High Energy Physics, NL-1009 DB Amsterdam, The Netherlands
[41] University of Notre Dame, Notre Dame, Indiana 46556, USA
[42] Ohio State University, Columbus, Ohio 43210, USA
[43] INFN Sezione di Padova[a]; Dipartimento di Fisica, Università di Padova[b], I-35131 Padova, Italy
[44] Laboratoire de Physique Nucléaire et de Hautes Energies, IN2P3/CNRS, Université Pierre et Marie Curie-Paris6, Université Denis Diderot-Paris7, F-75252 Paris, France
[45] INFN Sezione di Perugia[a]; Dipartimento di Fisica, Università di Perugia[b], I-06123 Perugia, Italy
[46] INFN Sezione di Pisa[a]; Dipartimento di Fisica, Università di Pisa[b]; Scuola Normale Superiore di Pisa[c], I-56127 Pisa, Italy
[47] Princeton University, Princeton, New Jersey 08544, USA
[48] INFN Sezione di Roma[a]; Dipartimento di Fisica, Università di Roma La Sapienza[b], I-00185 Roma, Italy
[49] Universität Rostock, D-18051 Rostock, Germany
[50] Rutherford Appleton Laboratory, Chilton, Didcot, Oxon, OX11 0QX, United Kingdom
[51] CEA, Irfu, SPP, Centre de Saclay, F-91191 Gif-sur-Yvette, France
[52] SLAC National Accelerator Laboratory, Stanford, California 94309 USA
[53] University of South Carolina, Columbia, South Carolina 29208, USA
[54] Southern Methodist University, Dallas, Texas 75275, USA
[55] Stanford University, Stanford, California 94305, USA
[56] State University of New York, Albany, New York 12222, USA
[57] Tel Aviv University, School of Physics and Astronomy, Tel Aviv, 69978, Israel
[58] University of Tennessee, Knoxville, Tennessee 37996, USA
[59] University of Texas at Austin, Austin, Texas 78712, USA
[60] University of Texas at Dallas, Richardson, Texas 75083, USA
[61] INFN Sezione di Torino[a]; Dipartimento di Fisica, Università di Torino[b], I-10125 Torino, Italy
[62] INFN Sezione di Trieste and Dipartimento di Fisica, Università di Trieste, I-34127 Trieste, Italy
[63] IFIC, Universitat de Valencia-CSIC, E-46071 Valencia, Spain
[64] Institute of Particle Physics[a]; University of Victoria[b], Victoria, British Columbia, Canada V8W 3P6
[65] Department of Physics, University of Warwick, Coventry CV4 7AL, United Kingdom
[66] University of Wisconsin, Madison, Wisconsin 53706, USA

We measure the mass difference, Δm_+, between the $D^*(2010)^+$ and the D^+ using the decay chain $D^*(2010)^+ \to D^+\pi^0$ with $D^+ \to K^-\pi^+\pi^+$. The data were recorded with the *BABAR* detector at

center-of-mass energies at and near the $\Upsilon(4S)$ resonance, and correspond to an integrated luminosity of approximately 468 fb^{-1}. We measure $\Delta m_+ = (140\,601.0 \pm 6.8[\text{stat}] \pm 12.9[\text{syst}])$ keV. We combine this result with a previous *BABAR* measurement of $\Delta m_0 \equiv m(D^*(2010)^+) - m(D^0)$ to obtain $\Delta m_D = m(D^+) - m(D^0) = (4\,824.9 \pm 6.8[\text{stat}] \pm 12.9[\text{syst}])$ keV. These results are compatible with and approximately five times more precise than the Particle Data Group averages.

PACS numbers: 13.20.Fc, 13.25Ft, 14.40.Lb, 12.38.Gc, 12.38.Qk, 12.39.Ki, 12.39.Pn

The difference between the masses of the D^0 and D^+ mesons [1], $\Delta m_D \equiv m(D^+) - m(D^0)$, is a key ingredient constraining calculations of symmetry breaking due to differing u and d quark masses and electromagnetic interactions in the frameworks of chiral perturbation theory [2] and lattice QCD [3]. Its value is reported by the Particle Data Group (PDG) [4] to be $\Delta m_D = (4.77 \pm 0.08)$ MeV. The most precise direct measurement, reported by the LHCb Collaboration, is $\Delta m_D = (4.76 \pm 0.12 \pm 0.07)$ MeV [5]. This was found by comparing the invariant mass distributions of $D^0 \to K^-K^+\pi^-\pi^+$ and $D^+ \to K^-K^+\pi^+$ decays. A more powerful constraint comes from the difference of measured $D^{*+} \to D^+\pi^0$ and $D^{*+} \to D^0\pi^+$ mass difference distributions. CLEO has previously reported $\Delta m_+ \equiv m(D^*(2010)^+) - m(D^+) = (140.64 \pm 0.08 \pm 0.06)$ MeV using the decay chain $D^{*+} \to D^+\pi^0$ with $D^+ \to K^-\pi^+\pi^+$ [6]. In the present paper we report a new measurement of Δm_+ and combine it with our previously measured $D^{*+} \to D^0\pi^+$ mass difference [7, 8], $\Delta m_0 \equiv m(D^*(2010)^+) - m(D^0)$, using two decay modes $D^0 \to K^-\pi^+$ and $D^0 \to K^-\pi^+\pi^-\pi^+$, to determine $\Delta m_D \equiv \Delta m_0 - \Delta m_+$ with very high precision.

This analysis is based on a data set corresponding to an integrated luminosity of approximately 468 fb^{-1} recorded at, and 40 MeV below, the $\Upsilon(4S)$ resonance [9]. The data were collected with the *BABAR* detector at the PEP-II asymmetric energy e^+e^- collider, located at the SLAC National Accelerator Laboratory. The *BABAR* detector is described in detail elsewhere [10, 11]. The momenta of charged particles are measured with a combination of a cylindrical drift chamber (DCH) and a 5-layer silicon vertex tracker (SVT), both operating within the 1.5 T magnetic field of a superconducting solenoid. Information from a ring-imaging Cherenkov detector is combined with specific ionization (dE/dx) measurements from the SVT and DCH to identify charged kaon and pion candidates. Electrons are identified, and photons from π^0 decays are measured, with a CsI(Tl) electromagnetic calorimeter (EMC). The return yoke of the superconducting coil is instrumented with tracking chambers for the identification of muons.

We study the $D^{*+} \to D^+\pi^0$ transition, using the $D^+ \to K^-\pi^+\pi^+$ decay mode, to determine the difference between the D^{*+} and D^+ masses Δm_+. To extract Δm_+, we fit the distribution of the difference between the reconstructed D^{*+} and D^+ masses, Δm. The signal component in the Δm fit is a resolution function determined from our Monte Carlo (MC) simulation of the detector response, while the contaminations from background are accounted for by a threshold function.

We suppress combinatorial backgrounds, and backgrounds with D^{*+} candidates from B decays, by requiring D^{*+} mesons produced in $e^+e^- \to c\bar{c}$ reactions to have momenta in the e^+e^- center-of-mass frame greater than 3.0 GeV. Background events from $D^{*+} \to D^0\pi^+$, with $D^0 \to K^-\pi^+\pi^0$, are vetoed by rejecting events for which the difference in the reconstructed masses $\Delta m' \equiv m(K^-\pi^+\pi^+\pi^0) - m(K^-\pi^+\pi^0)$ for each of the π^+ daughters is smaller than 160 MeV. This causes almost no signal loss. The decay chain is fitted subject to geometric constraints at the D^{*+} production vertex and the D^+ decay vertex, and to a kinematic constraint that the D^+ laboratory momentum points back to the interaction region. The χ^2 p-value from the fit is required to be greater than 0.1%.

The π^0 from D^{*+} decay has a laboratory momentum of about 300 MeV, and is referred to as the "slow pion" (π^0_s). The properties of the photons from from π^0_s decays, with energy below 500 MeV, energy resolution (σ_E/E) of about 7%, and angular resolutions (σ_θ, σ_ϕ) of about 10 mrad, are measured with large uncertainties. In the $\pi^0_s \to \gamma\gamma$ reconstruction, we first require both photon energies to be above 60 MeV, the total energy to be greater than 200 MeV, and the diphoton invariant mass to be between 120 MeV and 150 MeV (approximately $\pm 2.5\sigma$ around the nominal π^0 mass [4]). After the selection, each photon pair is kinematically fitted to the hypothesis of a π^0 originating from the event primary vertex, and with the diphoton mass constrained to the nominal π^0 mass. This greatly improves the reconstructed π^0 momentum resolution, and therefore the Δm resolution. The π^0 relative momentum resolution after the kinematic fit is $\sigma_p/p \sim 3\%$; this is still considerably worse than the approximately 0.5% D^+ relative momentum resolution.

Our MC simulation uses an energy calibration method that accounts for energy loss in the EMC differently than the energy calibration method that is used in data. This results in a reconstructed π^0 mass ($m_{\gamma\gamma}$) peak in MC events that is about 0.5 MeV below the nominal mass. In contrast, the $m_{\gamma\gamma}$ peak value from the calibrated data events generally coincides with the nominal value. Therefore, we approximate the neutral energy correction algorithm used in data in our MC simulated events, so that the reconstructed photon energies are rescaled with factors depending on photon energy and data-taking period.

This improves the agreement between data and simulation. However, we still find that in the simulated events, the reconstructed π^0 momentum remains slightly biased when compared with its generated value. To account for this bias, we additionally rescale the π^0 momentum in each simulated event by a factor of approximately 0.2%, depending on the diphoton opening angle.

Decay candidates $D^+ \to K^-\pi^+\pi^+$ are formed from well-measured tracks with kaon or pion particle identification and with a $K^-\pi^+\pi^+$ invariant mass $m_{K\pi\pi}$ within 1.86 and 1.88 GeV (approximately $\pm 2\sigma$ around the nominal D^+ mass [4]). This reduces background from random combinations of tracks, especially from $D^* \to D\pi_s^0$ decays with a correctly reconstructed π_s^0, which will also peak in the signal region of the Δm distribution. As in Ref. [7], we reject candidates with any D^+ daughter track for which the cosine of the polar angle measured in the laboratory frame $\cos\theta_t$ is above 0.89; this criterion reduces the final sample by approximately 10%. To further suppress peaking background events, we use a likelihood variable to select D^+ candidates, based on measured decay vertex separation from the primary vertex, and on Dalitz-plot position. This likelihood criterion rejects about 70% of background events with incorrectly reconstructed D^+, while retaining about 77% of signal events. Figure 1 shows the $m_{K\pi\pi}$ distribution for data events passing all selection criteria except for the requirement on $m_{K\pi\pi}$. For illustrative purposes, we fit the $m_{K\pi\pi}$ distribution by modeling the D^+ signal with a sum of two Gaussian functions sharing a common mean, and random background events with a linear function. After all selection criteria, the fraction of candidates with a correctly reconstructed D^+, as estimated from the $m_{K\pi\pi}$ fit, is about 95%.

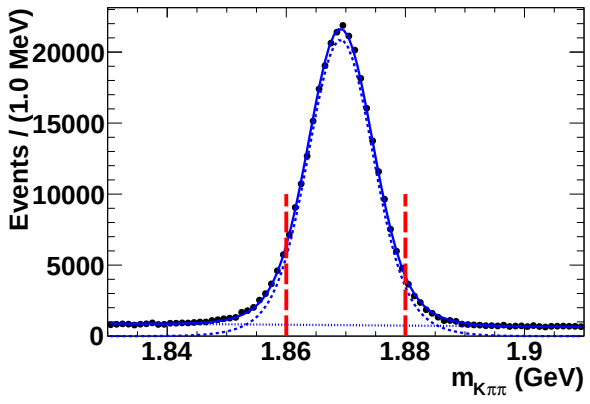

FIG. 1. (color online) The reconstructed D^+ mass distribution of real data, after all D^{*+} selection criteria except for the D^+ mass requirement, which is marked by the two vertical dashed lines. The result of the fit described in the text is superimposed (solid line), together with the background (dotted line) and signal (dashed line) components.

The value of Δm_+ is obtained from a fit to the Δm distribution in a two-step procedure as illustrated in Fig. 2 (a) and (b). First, we model the Δm resolution function by fitting the Δm distribution for correctly reconstructed signal MC events, using a sum of three Gaussian or Gaussian-like probability density functions (PDFs):

$$\begin{aligned}\mathcal{S}(\Delta m) &= f_1 \mathrm{G}(\Delta m; \Delta m_+ + \delta_{\Delta m_+}, \sigma_1) \\ &+ (1-f_1)\left[f_2 \mathrm{CB}(\Delta m; \Delta m_+ + \delta_{\Delta m_+}, \sigma_2, \alpha, n)\right. \\ &\left. +(1-f_2)\mathrm{BfG}(\Delta m; \Delta m_+ + \delta_{\Delta m_+}, \sigma_3^L, \sigma_3^R)\right] , \quad (1)\end{aligned}$$

where f_1 and f_2 give the fractions for the composite PDFs of G (Gaussian), CB (Crystal Ball [12], with α and n as two parameters to model the high mass tail), and BfG (a two-piece normal distribution with widths σ_3^L and σ_3^R on the left and right of $(\Delta m_+ + \delta_{\Delta m_+})$, respectively). The sum $(\Delta m_+ + \delta_{\Delta m_+})$ is therefore the common peak position of the three PDFs. In the fit to the high-statistics MC sample (Fig. 2(a)), Δm_+ is fixed at the generated value of 140.636 MeV, and $\delta_{\Delta m_+}$ is a measure of the possible bias induced by our event selection procedure, or the chosen form for the resolution function. The fit gives $\delta_{\Delta m_+} = (+16.6 \pm 2.5)$ keV, with the uncertainty from the limited size of our MC sample. The fit results for the shape parameters are shown in Fig. 2(a); and the full-width at half maximum (FWHM) of the resolution function is found to be about 2.1 MeV, which is mainly due to the resolution of the π_s^0.

The second step (Fig. 2(b)) is an unbinned maximum-likelihood fit to real data using the PDF from the first step to model signal, and a threshold function to model the combinatorial background [13]:

$$T(\Delta m; \kappa) = \Delta m \sqrt{u} \exp(\kappa \cdot u) , \quad (2)$$

where $u = (\Delta m / m_{\mathrm{endpt}})^2 - 1$, and κ is the slope parameter which is allowed to vary in the fit. We fix the end point m_{endpt} at the nominal π^0 mass [4] as the physical limit of Δm. In the data fit, we fix the bias $\delta_{\Delta m_+}$, fractions $f_{1,2}$, and CB tail parameters to the MC values from the first step, while allowing the widths $\sigma_{1,2,3}$ to be free in the fit to allow for differences between MC simulation and data. Figure 2(b) presents the data and the fit, with the normalized residuals showing good data and fit agreement. There are $150\,893 \pm 623$ signal events, the observed FWHM of the signal shape is about 2.0 MeV, and we determine $\Delta m_+ = (140\,597.6 \pm 6.8)$ keV, where the uncertainty is statistical only (σ_{stat}). A bias correction to this result will be discussed later.

We estimate systematic uncertainties on Δm_+ from a variety of sources. Separately, we study the Δm_+ dependence on the D^{*+} laboratory momentum p_{lab}, on the cosine of D^{*+} laboratory polar angle $\cos\theta$, on the D^{*+} laboratory azimuthal angle ϕ, on $m_{K\pi\pi}$, and on the diphoton opening angle $\theta_{\gamma\gamma}$ from $\pi^0 \to \gamma\gamma$, by collecting

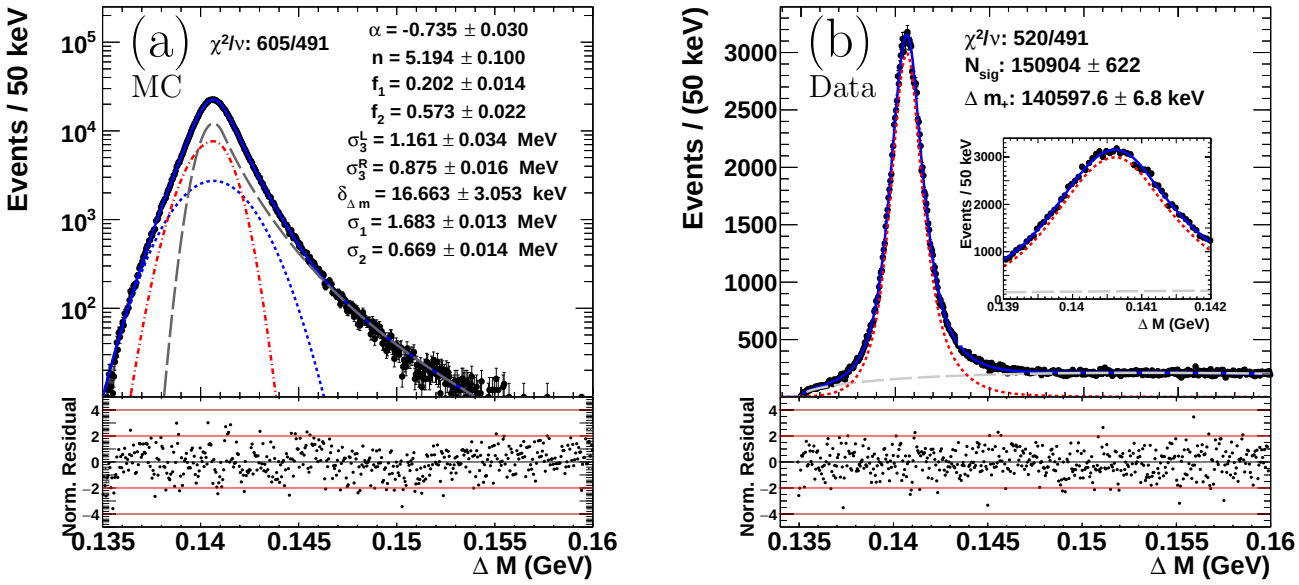

FIG. 2. (color online) Left: Δm fit to correctly reconstructed signal MC events. Shown are the total fit (blue solid line), Crystal Ball function (gray long-dashed line), Gaussian (blue short-dashed line), and two-piece normal distribution function (red dash-dotted line). The fitted signal shape parameters defined in Eq. 1 are also shown in the text box. Right: Δm fit to real data. Shown are the total fit (blue solid line), signal PDF (magenta short-dashed line), and background PDF (gray long-dashed line). The inset shows the fit around the peak region. The Δm_+ central value from the fit is later corrected by the estimated fit bias. Normalized residuals shown underneath both fit plots are defined as $(N_{\rm observed} - N_{\rm predicted})/\sqrt{N_{\rm predicted}}$.

fit results for Δm_+ in 10 subsets of data with roughly equal statistics for each parameter. Furthermore, we divide our data into four disjoint subsets of data-taking periods. For the data fit in each subset, the value of $\delta_{\Delta m_+}$ is determined separately from signal MC events with the same event selection criteria as for that subset. This is meant to expose possible detector response effects that have not been modeled in the simulation. We search for variations larger than those expected from statistical fluctuations based on a method similar to the PDG scale factor [4, 8]. If the fit results from a given dependence study are compatible with a constant value, in the sense that $\chi^2/\nu < 1$, where ν is the number of degrees of freedom, we assign no systematic uncertainty. In the case that $\chi^2/\nu > 1$, we ascribe an uncertainty of $\sigma_{\rm sys} = \sigma_{\rm stat}\sqrt{\chi^2/\nu - 1}$ to account for unidentified detector effects. We observe $\chi^2/\nu > 1$ in the cases of $p_{\rm lab}$, $\cos\theta$ and $\theta_{\gamma\gamma}$ (shown in Fig. 3 in [14]). Systematic uncertainties of 5.0 keV, 6.9 keV, and 6.1 keV are assigned for the D^{*+} $p_{\rm lab}$, D^{*+} $\cos\theta$, and $\theta_{\gamma\gamma}$ dependences, respectively, for which the p-values for the null hypotheses are 0.12, 0.03, and 0.06. The p-values for the variations with D^{*+} azimuthal angle and D^+ mass are 0.99 and 0.47, and no systematic uncertainties are assigned for these observations.

The five signal shape parameters α, n, $f_{1,2}$, and $\delta_{\Delta m_+}$, determined from the fit to signal MC events (Fig. 2 (a)), possess statistical uncertainties that are highly correlated. We account for their uncertainties and correlations by producing 100 sets of correlated random numbers of signal shape parameters based on the central values and the covariance matrix from the fit to signal MC events. Then for each set, we rerun the data fit by fixing α, n, $f_{1,2}$, and $\delta_{\Delta m_+}$ to the corresponding random numbers in the set. The distribution of the 100 fit values for Δ_{m_+} has a root mean square of 2.1 keV which is taken as systematic uncertainty for the signal shape parameters.

To test whether our fit procedure introduces a bias on Δm_+, we generate an ensemble of data sets with signal and background events generated from appropriately normalized PDFs based on our nominal data fit. The data sets are then fitted with exactly the same fit model as for real data ("pure pseudoexperiment"). By performing 500 pseudoexperiments, we collect Δm_+ pulls, defined as the differences of fitted and input values normalized by the fitted errors. The mean of the pulls is $-(50 \pm 4)\%$, while the root mean square is consistent with being unity. We thus correct for the bias in our fit model by adding $50\% \times \sigma_{\rm stat} = 3.4$ keV to the fit value of Δm_+ from the data, and assign a systematic uncertainty equal to half this bias correction (1.7 keV). We perform another type of pseudoexperiment by fitting to ensembles of data sets where signal and background events are produced by randomly sampling the corresponding simulated events. In this case, the peaking background is included as part of the background events. The collected

TABLE I. Assigned systematic errors from all considered sources.

Source	Δm_+ systematic [keV]
Fit bias	1.7
D^{*+} $p_{\rm lab}$ dependence	5.0
D^{*+} $\cos\theta$ dependence	6.9
D^{*+} ϕ dependence	0.0
$m(D^+_{\rm reco})$ dependence	0.0
Diphoton opening angle dependence	6.1
Run period dependence	0.0
Signal model parametrization	2.1
EMC calibration	7.0
MC π^0 momentum rescaling	0.5
Total	12.9

pulls show a mean fit bias consistent with that found in our pure pseudoexperiments, and we assign no systematic uncertainty related to the peaking background.

To account for the systematic uncertainty due to imperfect photon energy calibration, we rescale photon energies in simulated signal events by $+0.3\%$ and -0.3%, and take the larger of the two variations in the Δm peak position, 7.0 keV, as the corresponding systematic uncertainty. We also take into account the associated uncertainties on the π^0 momentum rescaling factors due to the limited size of our MC sample, and find the related systematic uncertainty to be 0.5 keV.

Besides the systematic studies, we also perform a series of consistency checks that are not used to assess systematics but rather to reassure us that the experimental approach and fitting technique behave reasonably. We vary the upper limit of the Δm fit range from its default position of 0.160 GeV to a series of values between 0.158 and 0.168 GeV. Also, we vary the selection criteria on the invariant masses $m_{K\pi\pi}$ and $m_{\gamma\gamma}$, as well as the Dalitz-plot based likelihood. The resulting fit values of Δm_+ from all these checks are consistent.

All systematic uncertainties of Δ_{m_+} are summarized in Table I; adding them in quadrature leads to a total of 12.9 keV. After adding the fit bias of 3.4 keV, our final result is $\Delta m_+ \equiv m(D^{*+}) - m(D^+) = (140\,601.0 \pm 6.8[\text{stat}] \pm 12.9[\text{syst}])$ keV. This result is consistent with the current world average of (140.66 ± 0.08) MeV, and about five times more precise. Combining with the *BABAR* measurement of $\Delta m_0 = (145\,425.9 \pm 0.5[\text{stat}] \pm 1.8[\text{syst}])$ keV based on the same data set, we obtain the D meson mass difference of $\Delta m_D = (4\,824.9 \pm 6.8[\text{stat}] \pm 12.9[\text{syst}])$ keV. This result is, as for Δm_+, about a factor of five more precise than the current world average, (4.77 ± 0.08) MeV. Adding the statistical and systematic uncertainties in quadrature, $\Delta m_D = (4\,824.9 \pm 14.6)$ keV. This can be compared with the corresponding values for the pion and kaon systems, $\Delta m_\pi = (4\,539.6 \pm 0.5)$ keV and $\Delta m_K = (-3\,934 \pm 20)$ keV [4].

We are grateful for the excellent luminosity and machine conditions provided by our PEP-II colleagues, and for the substantial dedicated effort from the computing organizations that support *BABAR* . The collaborating institutions wish to thank SLAC for its support and kind hospitality. This work is supported by DOE and NSF (USA), NSERC (Canada), CEA and CNRS-IN2P3 (France), BMBF and DFG (Germany), INFN (Italy), FOM (The Netherlands), NFR (Norway), MES (Russia), MINECO (Spain), STFC (United Kingdom), BSF (USA-Israel). Individuals have received support from the Marie Curie EIF (European Union) and the A. P. Sloan Foundation (USA).

* Now at: Wuhan University, Wuhan 43072, China
† Now at: Università di Bologna and INFN Sezione di Bologna, I-47921 Rimini, Italy
‡ Deceased
§ Now at: University of Huddersfield, Huddersfield HD1 3DH, UK
¶ Now at: University of South Alabama, Mobile, Alabama 36688, USA
** Also at: Università di Sassari, I-07100 Sassari, Italy

[1] Charge conjugation is implied throughout this paper.
[2] J. L. Goity and C. P. Jayalath, Phys. Lett. **B650**, 22 (2007).
[3] R. Horsley *et al.* (QCDSF Collaboration), PoS **Lattice2013**, 499 (2014).
[4] C. Patrignani *et al.* (Particle Data Group), Chin. Phys. **C40**, 100001 (2016).
[5] R. Aaij *et al.* (LHCb Collaboration), JHEP **06**, 065 (2013).
[6] D. Bortoletto *et al.* (CLEO Collaboration), Phys. Rev. Lett. **69**, 2046 (1992).
[7] J. P. Lees *et al.* (*BABAR* Collaboration), Phys. Rev. Lett. **111**, 111801 (2013).
[8] J. P. Lees *et al.* (*BABAR* Collaboration), Phys. Rev. **D 88**, 052003 (2013), [Erratum: Phys. Rev. **D 88**, 079902 (2013)].
[9] J. P. Lees *et al.* (*BABAR* Collaboration), Nucl. Instr. Meth. Phys. Res., Sect. A **726**, 203 (2013).
[10] B. Aubert *et al.* (*BABAR* Collaboration), Nucl. Instr. Methods Phys. Res., Sect. A **479**, 1 (2002).
[11] B. Aubert *et al.* (*BABAR* Collaboration), Nucl. Instr. Meth. Phys. Res., Sect. A **729**, 615 (2013).
[12] M. J. Oreglia, Ph.D. thesis, Stanford University Report No. SLAC-R-236, 1980; J. E. Gaiser, Ph.D. thesis, Stanford University Report No. SLAC-R-255, 1982; T. Skwarnicki, Ph.D. thesis, Cracow Institute of Nuclear Physics Report No. DESY-F31-86-02, 1986.
[13] H. Albrecht *et al.* (ARGUS Collaboration), Z. Phys. **C48**, 543 (1990).
[14] Additional plots are available through EPAPS Document No. E-PRLTAO-XX-XXXXX. For more information on EPAPS, see http://www.aip.org/pubservs/epaps.html.

EPAPS MATERIAL

The following includes supplementary material for the Electronic Physics Auxiliary Publication Service.

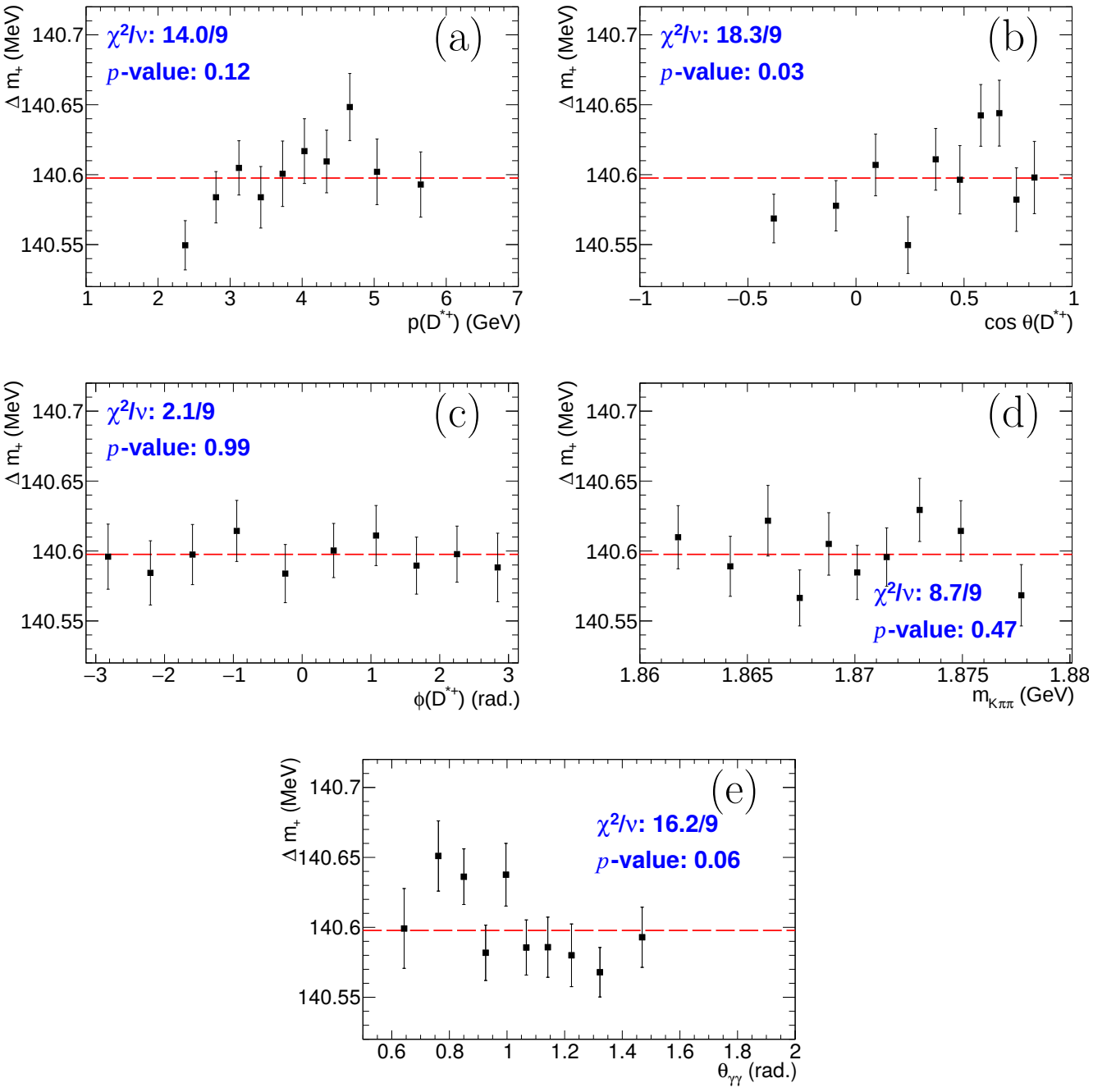

FIG. 3. (color online) Δm_+ measurements as functions of different D^{*+} properties: (a) momentum magnitude $p(D^{*+})$, (b) polar angle $\cos\theta$, (c) azimuthal angle ϕ, (d) $m_{K\pi\pi}$, and (e) π^0 opening angle $\theta_{\gamma\gamma}$. In each plot we fit the results with a constant and the fitted χ^2/ν with associated p-value is shown in each plot. The red dashed lines mark the Δm_+ central value from our nominal fit.